

## Understanding the Rapid Precipitation Response to CO<sub>2</sub> and Aerosol Forcing on a Regional Scale\*

THOMAS B. RICHARDSON AND PIERS M. FORSTER

*School of Earth and Environment, University of Leeds, Leeds, United Kingdom*

TIMOTHY ANDREWS

*Met Office Hadley Centre, Exeter, United Kingdom*

DOUG J. PARKER

*School of Earth and Environment, University of Leeds, Leeds, United Kingdom*

(Manuscript received 4 March 2015, in final form 14 October 2015)

### ABSTRACT


Precipitation exhibits a significant rapid adjustment in response to forcing, which is important for understanding long-term climate change. In this study, fixed sea surface temperature (SST) simulations are used to analyze the spatial pattern of the rapid precipitation response. Three different forcing scenarios are investigated using data obtained from phase 5 of CMIP (CMIP5): an abrupt quadrupling of CO<sub>2</sub>, an abrupt increase in sulfate, and an abrupt increase in all anthropogenic aerosol levels from preindustrial to present day. Analysis of the local energy budget is used to understand the mechanisms that drive the observed changes.

It is found that the spatial pattern of the rapid precipitation response to forcing is primarily driven by rapid land surface temperature change, rather than the change in tropospheric diabatic cooling. As a result, the pattern of response due to increased CO<sub>2</sub> opposes that due to sulfate and all anthropogenic aerosols, because of the opposing surface forcing. The rapid regional precipitation response to increased CO<sub>2</sub> is robust among models, implying that the uncertainty in long-term changes is mainly associated with the response to SST-mediated feedbacks. Increased CO<sub>2</sub> causes rapid warming of the land surface, which destabilizes the troposphere, enhancing convection and precipitation over land in the tropics. Precipitation is reduced over most tropical oceans because of a weakening of overturning circulation and a general shift of convection to over land. Over most land regions in the midlatitudes, circulation changes are small. Reduced tropospheric cooling therefore leads to drying over many midlatitude land regions.

### 1. Introduction

Regional precipitation change is one of the most uncertain aspects of climate change prediction (Stephens et al. 2010; Liepert and Previdi 2012; Stevens and Bony

2013) and can have major societal implications (Wake 2013). On a global scale, the precipitation response to a forcing can be understood through atmospheric energy budget arguments (Mitchell et al. 1987; Allen and Ingram 2002; O’Gorman et al. 2012). Tropospheric radiative cooling tightly constrains global precipitation (Pendergrass and Hartmann 2014), leading to a slow sea surface temperature (SST)-dependent response due to radiative feedbacks (Previdi 2010) and a forcing-dependent rapid adjustment (or fast response) due to the near-instantaneous change in atmospheric cooling (Lambert and Faull 2007; Bala et al. 2010; Andrews et al. 2010; Kvalevåg et al. 2013; Kravitz et al. 2013). The rapid

 Denotes Open Access content.

\* Supplemental information related to this paper is available at the Journals Online website: <http://dx.doi.org/10.1175/JCLI-D-15-0174.s1>.

*Corresponding author address:* Thomas B. Richardson, School of Earth and Environment, University of Leeds, Leeds LS2 9JT, United Kingdom.  
E-mail: eetbr@leeds.ac.uk



This article is licensed under a [Creative Commons Attribution 4.0 license](https://creativecommons.org/licenses/by/4.0/).

adjustment is vital for understanding the different hydrological sensitivities between forcing agents (Andrews and Forster 2010; Andrews et al. 2010; Cao et al. 2011).

On a regional scale, precipitation changes are more difficult to predict because of complex variations in circulation patterns (Bony et al. 2013). Many studies on regional precipitation have utilized the water vapor budget (Emori 2005; Bony et al. 2013; Huang et al. 2013) to analyze change. There has been very little previous work on understanding the regional drivers of precipitation as a response to forcing. However, local precipitation change can be understood in a similar fashion to global change, through incorporating horizontal dry static energy transport into the atmospheric energy budget (Muller and O’Gorman 2011). The local energy budget provides a simple framework for analyzing the regional precipitation response to forcing.

It has been shown that increasing CO<sub>2</sub> levels produces a significant rapid reduction in precipitation (Mitchell et al. 1987; Andrews et al. 2010), which exhibits substantial spatial variation (Bony et al. 2013; Chadwick et al. 2014). Bony et al. (2013) showed that around half the 30-yr mean change in tropical overturning circulation due to quadrupling CO<sub>2</sub> occurs within the first five days, driving much of the tropical precipitation pattern. The rapid adjustment makes an important contribution to long-term precipitation change, and therefore it is important to understand the mechanisms involved.

The rapid tropical precipitation response is likely affected by land surface temperature adjustments influencing atmospheric stability (Cao et al. 2012; Chadwick et al. 2014) and reduced tropospheric radiative cooling affecting general circulation (Bony et al. 2013). However, it is not well established which of these mechanisms is the principal driver of the spatial pattern. In addition, it is not known what mechanisms drive the precipitation pattern outside of the tropics. In this study, we utilize the local energy budget framework to help understand the spatial pattern of rapid precipitation adjustments. We use idealized experiments from phase 5 of the Coupled Model Intercomparison Project (CMIP5) to investigate the mechanisms driving the regional rapid precipitation response to CO<sub>2</sub> and aerosol forcing.

## 2. Methods

### a. Data and experiments

There are three methods available to isolate the rapid precipitation adjustment: fixed sea surface temperature experiments, regression, or using the first year of fully coupled simulations. However, regression is noisy on a

regional scale, and using the first year of coupled simulations incorporates a significant amount of SST change (Sherwood et al. 2014). Therefore, we chose to isolate the rapid adjustment using 30-yr fixed SST experiments, in which only the land surface and atmosphere are allowed to adjust. In these simulations, SSTs and sea ice are prescribed using data from preindustrial control runs, thus suppressing any feedbacks mediated by SST change. Vegetation maps for land are also prescribed, but the vegetation may respond (e.g., through stomatal opening or leaf area index) (Taylor et al. 2009).

Data were obtained from models participating in CMIP5 (see Table A1). We analyze the precipitation response to three different forcing scenarios: an abrupt quadrupling of CO<sub>2</sub> levels (sstClim4xCO<sub>2</sub>), an abrupt increase of sulfate levels from preindustrial to present day (sstClimSulfate), and an abrupt increase of all anthropogenic aerosol from preindustrial to present day (sstClimAerosol). The models analyzed in this study represent the effects of aerosols in varying detail, as shown in Table S1 in the supplementary information (Allen et al. 2015). Changes in climate variables were calculated by subtracting the 30-yr mean of control runs from the 30-yr mean of forced runs. Multimodel mean errors are taken as the 5%–95% uncertainty range assuming a normal distribution.

### b. Global and local atmospheric energy budget

We utilize both the global and local atmospheric energy budgets to help understand the precipitation response to forcing. Globally the latent heat released by precipitation is balanced by the longwave (LW) and shortwave (SW) cooling of the troposphere and the surface sensible heat flux (SH) (O’Gorman et al. 2012). Following Muller and O’Gorman (2011), we decompose regional precipitation  $P$  by incorporating dry static energy flux divergence  $H$  into the global budget, as shown in Eq. (1):

$$L_c \delta P = \delta Q + \delta H = \delta LW + \delta SW - \delta SH + \delta H, \quad (1)$$

where  $L_c$  is the latent heat of condensation,  $Q$  is the diabatic cooling of the troposphere (excluding latent heat), and  $\delta$  denotes the perturbation between climates. Change in  $H$  is given by the sum of mean  $H_m$  and eddy  $H_{\text{trans}}$  components. The total change in  $H$  and  $H_{\text{trans}}$  are calculated as residuals. The change in  $H_m$  is calculated as the sum of components due to advection across horizontal  $H_{\text{hor}}$ , and vertical  $H_{\text{vert}}$  gradients of mean dry static energy, as shown in Eq. (2):

$$\delta H_m = \delta H_{\text{hor}} + \delta H_{\text{vert}} = \delta \int \mathbf{u} \cdot \nabla \bar{s} + \delta \int \bar{\omega} \frac{\partial \bar{s}}{\partial p}, \quad (2)$$

where  $\mathbf{u}$  is the horizontal velocity,  $s$  is dry static energy,  $\omega$  is the vertical velocity, and  $p$  is pressure. Integral signs

represent mass-weighted integration over the column, and overbars denote climate means. The horizontal-advective term is further decomposed into components associated with changes in horizontal winds  $H_u$ , and changes in horizontal gradients of dry static energy  $H_s$ , as shown in Eq. (3):

$$\delta H_{\text{hor}} = \delta H_u + \delta H_s = \int \delta[\bar{\mathbf{u}}] \cdot \nabla \bar{s} + \int \bar{\mathbf{u}} \cdot \delta[\nabla \bar{s}]. \quad (3)$$

The vertical component is decomposed into a thermodynamic term  $H_{\text{therm}}$ , associated with changes in the vertical gradient of dry static energy, and a dynamic term  $H_{\text{dyn}}$  associated with changes in mean vertical velocity [Eq. (4)]:

$$\delta H_{\text{vert}} = \delta H_{\text{dyn}} + \delta H_{\text{therm}} = \int \delta[\bar{\omega}] \frac{\partial \bar{s}}{\partial p} + \int \bar{\omega} \delta \left[ \frac{\partial \bar{s}}{\partial p} \right]. \quad (4)$$

All energy budget terms are converted into precipitation units ( $\text{mm yr}^{-1}$ ).

### 3. Results and discussion

#### a. Global mean adjustment

Figure 1 shows the multimodel mean globally averaged precipitation and atmospheric energy budget response for the three forcing scenarios. The dominant effect of quadrupling  $\text{CO}_2$  (Fig. 1a) is a strong reduction in LW cooling at the top of the atmosphere (TOA), and a smaller magnitude increase in downwelling LW radiation at the surface, producing a net increase in atmospheric absorption. Overall, the diabatic cooling of the troposphere is reduced by  $-51.28 \pm 14.7 \text{ mm yr}^{-1}$ , and is balanced by a global mean reduction in precipitation of  $-50.02 \pm 14.4 \text{ mm yr}^{-1}$ . This is consistent with previous studies showing rapid reductions in global mean precipitation following increased  $\text{CO}_2$  (Andrews et al. 2010; Cao et al. 2012; Kvalevåg et al. 2013). The reduction is significant in comparison to the feedback response, which is currently estimated at around  $20\text{--}30 \text{ mm yr}^{-1} \text{ K}^{-1}$  ( $2\%\text{--}3\% \text{ K}^{-1}$ ) (Andrews et al. 2010).

For increased sulfate levels, the dominant effect is a decrease in the net downwelling SW radiation at both the TOA and surface, resulting in a negligible change in global mean tropospheric cooling and precipitation (Fig. 1b). This is consistent with previous global mean studies (Andrews et al. 2010; Kvalevåg et al. 2013). Increasing all anthropogenic aerosol levels also mainly affects the SW radiative fluxes (Fig. 1c). In addition to the sulfate effects, black carbon causes increased SW absorption in the troposphere. Because of the black carbon, global mean tropospheric cooling is reduced

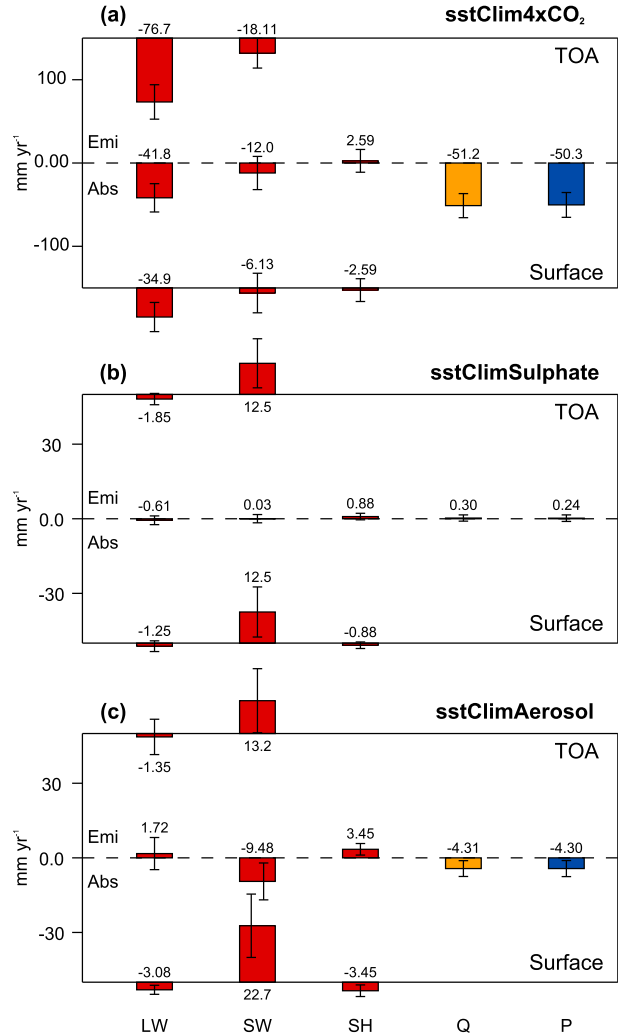


FIG. 1. Multimodel mean energy budget response at the TOA (upper line) and surface (lower line), and the net result for the troposphere (middle dashed line) for (a) sstClim4xCO<sub>2</sub>, (b) sstClimSulfate, and (c) sstClimAerosol. The columns depict change in longwave radiation, shortwave radiation, sensible heat flux, tropospheric diabatic cooling, and precipitation (all converted to  $\text{mm yr}^{-1}$ ). All values are positive upward at the TOA and surface. For the troposphere, positive values represent increased net emission (Emi) of energy, and negative values represent net absorption (Abs) of energy. Error bars represent the 5%–95% uncertainty assuming a normal distribution.

by  $-4.31 \pm 3.2 \text{ mm yr}^{-1}$  and precipitation by  $-4.30 \pm 3.2 \text{ mm yr}^{-1}$ . The changes in tropospheric cooling due to the different forcing agents tightly constrain the global mean rapid precipitation adjustment across the models, in agreement with previous work (Andrews et al. 2010; Kvalevåg et al. 2013).

#### b. Regional adjustment

The precipitation response to quadrupling  $\text{CO}_2$  exhibits a robust spatial pattern across models, with

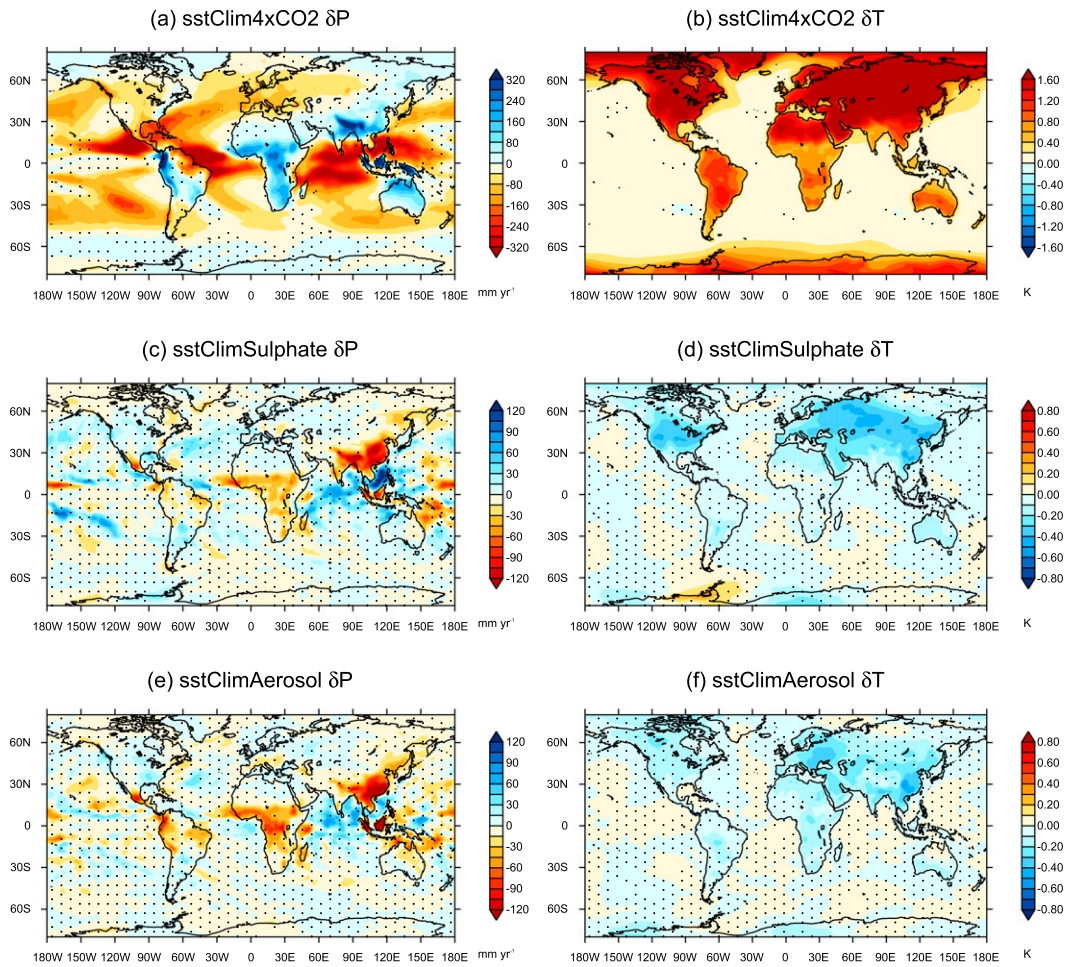


FIG. 2. Multimodel mean precipitation  $P$  ( $\text{mm yr}^{-1}$ ) change for (a) sstClim4xCO<sub>2</sub>, (c) sstClimSulfate, and (e) sstClimAerosol simulations. Multimodel mean near-surface air temperature  $T$  (K) change for (b) sstClim4xCO<sub>2</sub>, (d) sstClimSulfate, and (f) sstClimAerosol. Stippling indicates where less than 80% of the models agree on sign. The color scale is reversed for (left) precipitation and (right) temperature such that blue represents increased precipitation and reduced temperature. Also note the changes in magnitude of color scales between experiments.

disagreement in sign mainly confined to regions of negligible change (Fig. 2a). The most prominent features are observed in the tropics, with significant reductions in regions of climatological large-scale ascent over the Indian Ocean, equatorial Atlantic, and western and eastern Pacific. Conversely, significant increases are observed over southern Asia, the Maritime Continent, Australia, Africa, and western South America. Figure 3a shows the mean precipitation response in the midlatitudes and tropics over land and sea for all models. It can be seen that, excluding one outlier, all the models agree on the sign of the change for each region, further demonstrating the robustness of the precipitation response. The robust spatial pattern implies uncertainty in long-term predictions is mainly associated with the response to SST-driven feedbacks (Ma and Xie 2013).

There is a significant shift of precipitation from over oceans to over land (Fig. 3a), with a mean increase of  $15.3 \pm 32.4 \text{ mm yr}^{-1}$  over land and a decrease of  $-81.4 \pm 19.7 \text{ mm yr}^{-1}$  over oceans (Table 1). This land-sea contrast indicates the importance of the rapid land surface adjustment to increasing CO<sub>2</sub>. The increased downwelling LW radiation due to increased CO<sub>2</sub> levels causes rapid warming of the land surface (Fig. 2b). Over land, there is an increase in mean near-surface air temperature of  $1.22 \pm 0.4 \text{ K}$ , which tends to destabilize the troposphere, enhancing convection and precipitation. The contrast in precipitation change is most prominent in the tropics (Fig. 3a), where precipitation increases by  $54.6 \pm 60.2 \text{ mm yr}^{-1}$  over land, and decreases by  $-111.6 \pm 30.1 \text{ mm yr}^{-1}$  over the sea. A similar land-sea contrast in precipitation is observed in the first month of fully coupled simulations with increased CO<sub>2</sub> (Cao

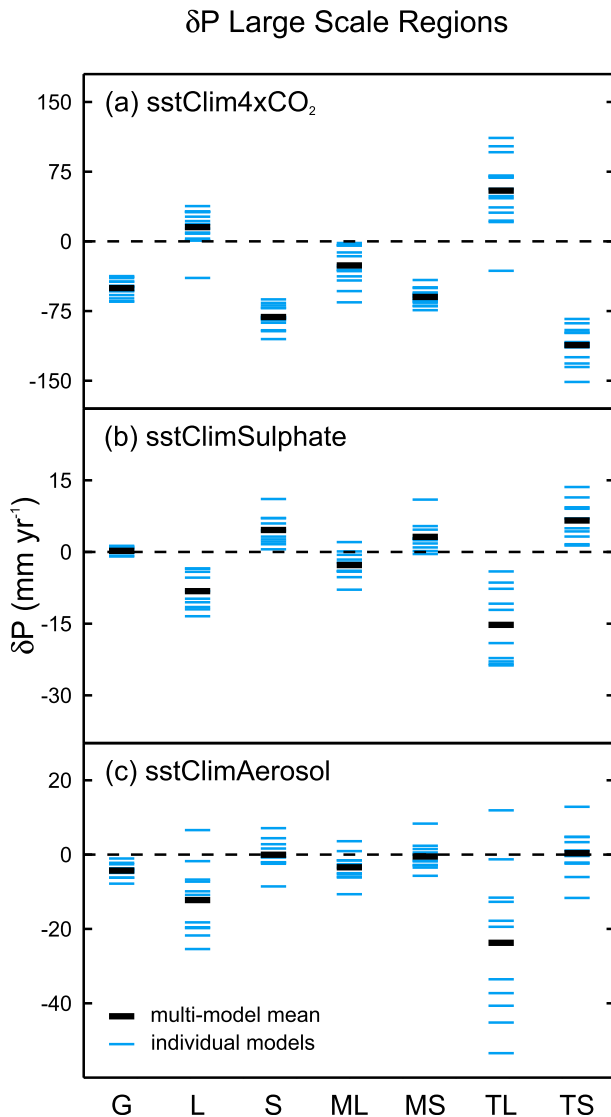


FIG. 3. Mean precipitation change ( $\text{mm yr}^{-1}$ ) over the globe (G), land (L), sea (S), midlatitude land (ML), midlatitude sea (MS), tropical land (TL), and tropical sea (TS) for (a) sstClim4xCO<sub>2</sub>, (b) sstClimSulphate, and (c) sstClimAerosol. Black lines indicate multi-model mean values, and blue lines indicate individual model values.

et al. 2012). The enhanced land–sea temperature contrast strengthens the African and Asian summer monsoons. However, there are large regions over land, predominantly in the midlatitudes, for which precipitation decreases. Notably, precipitation also decreases in the northeastern of South America.

The sstClimSulphate and sstClimAerosol multimodel mean precipitation adjustments exhibit very similar spatial patterns to one another (Figs. 2c,e). Significant reductions in precipitation occur over Africa, southern Asia, and the Maritime Continent. There is a shift of precipitation from land to sea for both simulations (see Table 1), most

prominent in the tropics (Figs. 3b,c). The precipitation pattern shown in both the sulfate and aerosol simulations is clearly opposed to that observed in the CO<sub>2</sub> experiment. Given the lack of opposing tropospheric forcing (see Fig. 1), this indicates that the surface forcing is the principal driver of the precipitation pattern through influencing land surface temperatures. The reduced downwelling SW radiation at the surface in both the aerosol experiments causes cooling of the land (Figs. 2d,f) and therefore tends to increase atmospheric stability over land regions. The small difference between the sstClimSulphate and sstClimAerosol global mean tropospheric forcing and precipitation (Fig. 1) has little effect on the spatial pattern, as the regional changes induced by the land surface adjustment are significantly larger in magnitude. The feedback responses of precipitation to increased greenhouse gases and reduced aerosols have also been shown to project onto similar spatial patterns to one another because of similar SST pattern change (Xie et al. 2013).

The largest reduction in precipitation for the sstClimSulphate and sstClimAerosol simulations occurs over southern Asia. This is consistent with Ganguly et al. (2012), who found that the rapid adjustment to increased aerosol of one model exhibited significant reductions in precipitation over Southeast Asia. Reducing the land–sea surface temperature contrast weakens the South Asian summer monsoon. The reduction in precipitation over Africa and southern Asia is fairly consistent between models (Figs. 2c,e). However, over most of the globe there is significantly more variability between models in the sstClimSulphate and sstClimAerosol simulations, most likely because the forcing at the TOA and surface is significantly less than for the CO<sub>2</sub> experiment. The resulting change in precipitation is therefore small relative to natural internal variability.

Aerosols can also affect precipitation through their role as cloud condensation and ice nuclei. The spatial pattern of precipitation change for the aerosol experiments is very similar between models that include aerosol effects on precipitation efficiency (second indirect effect) and those that do not (Figs. S5 and S6 in the supplementary information). This indicates that the radiative effects primarily drive the spatial pattern of precipitation change. The second indirect effect may enhance the spatial pattern through further reducing precipitation over tropical land regions. For the sstClimAerosol simulation, the cloud albedo effect contributes significantly to the changes in land surface temperature and precipitation pattern (Fig S6).

#### c. $4 \times \text{CO}_2$ local energy budget

To understand the mechanisms driving the regional rapid precipitation adjustment to increased CO<sub>2</sub> in more

TABLE 1. Multimodel mean precipitation  $P$ , tropospheric diabatic cooling  $Q$ , and land surface temperature  $T$  response. Errors represent the 5%–95% uncertainties assuming a normal distribution.

Experiment	Global mean $\delta P$ (mm yr <sup>-1</sup> )	Global mean $\delta Q$ (mm yr <sup>-1</sup> )	Land mean $\delta P$ (mm yr <sup>-1</sup> )	Sea mean $\delta P$ (mm yr <sup>-1</sup> )	Land mean $\delta T$ (K)
sstClim4xCO <sub>2</sub>	-50.3 ± 14.9	-51.2 ± 14.5	15.3 ± 32.4	-81.4 ± 19.7	1.22 ± 0.4
sstClimSulfate	0.24 ± 1.3	0.30 ± 1.3	-8.19 ± 6.3	4.59 ± 5.3	-0.13 ± 0.1
sstClimAerosol	-4.30 ± 3.2	-4.31 ± 3.2	-12.2 ± 15.9	-0.03 ± 6.8	-0.11 ± 0.1

detail, we analyze the local energy budget response of one model, HadGEM2-A. The rapid precipitation response and tropospheric energy budget components are shown in Fig. 4. The dry static energy flux divergence components are shown in Fig. 5. The spatial pattern of the precipitation response (Fig. 4a) is very consistent with the multimodel mean response (Fig. 2a).

The change in dry static energy flux divergence  $H$  (Fig. 4b) accounts for most of the large regional variations observed within the tropics and exhibits a clear land–sea contrast. The contribution from transient eddies (Fig. 5b) is small relative to that by mean motions (Fig. 5a), particularly in the tropics. The thermodynamic component (Fig. 5d) is negligible over much of the globe because of the fixed SSTs. The dynamic component, associated with changes in mean vertical velocity (Fig. 5c), dominates the adjustment in  $H$  in the tropics. Bony et al. (2013) similarly found that the first year tropical precipitation response in fully coupled simulations is dominated by changes in circulation patterns. Over most land areas  $\delta H_{\text{dyn}}$  is positive, with notable exceptions over northeastern South America and northern Asia. This indicates enhanced convection over land regions, due to increased land surface temperatures, destabilizing the troposphere. Over the ocean, in regions of large-scale ascent there are large reductions in  $H_{\text{dyn}}$ . In contrast, in descent regions,  $H_{\text{dyn}}$  generally increases. This implies an overall weakening of overturning circulation, coupled with a shift of convection to over land. This is consistent with the rapid circulation response observed in fully coupled simulations (Bony et al. 2013).

Outside of the tropics, the horizontal-advective components  $H_u$  and  $H_s$  (Figs. 5e,f) become more significant because of the large meridional dry static energy gradients. The spatial patterns of changes in  $H_u$  and  $H_s$  are generally opposed; however, the magnitude of changes in  $H_u$  is significantly larger. The net effect is that changes in horizontal advection of dry static energy counteract the dynamic component (Fig. 5c). As a result, changes in horizontal energy transport are reduced in the mid-to-high latitudes. Therefore, this reduces the magnitude of precipitation changes required for energy balance.

Over much of the globe, the tropospheric cooling is reduced (Fig. 4c), contributing to a decrease in precipitation and dominating the global mean. The reduction is mainly due to increased absorption of LW radiation by CO<sub>2</sub> (Fig. 4e), as well as increased SH flux from the surface over many land areas (Fig. 4d). The change in SW cooling is negligible over most of the globe (Fig. 4f).

The change in cloud fraction, atmospheric cloud radiative effect (CRE), and radiative fluxes at the TOA and surface are shown in Fig. 6. The CRE is defined as the difference between net radiative fluxes out of the troposphere in all-sky and clear-sky conditions. The change in CRE includes “cloud masking” effects (Soden et al. 2004). CRE changes (Fig. 6a) strongly influence the spatial pattern of the LW tropospheric cooling (Fig. 4e) (Lambert et al. 2014). In the tropics,  $\delta \text{CRE}$  (Fig. 6a) and  $\delta H_{\text{dyn}}$  (Fig. 5c) are strongly negatively correlated ( $r = -0.85$ ). In regions where  $\delta H_{\text{dyn}}$  is positive, indicating enhanced convection, there is decreased radiative cooling because of clouds. Conversely, in regions with negative  $\delta H_{\text{dyn}}$ , there is increased radiative cooling because of clouds. This effect slightly dampens the large regional variations driven by circulation changes in the tropics.

Over most land in the midlatitudes (North and South America, Europe, and western/central Asia), where  $\delta H$  is small, the change in tropospheric cooling dominates the precipitation response (Fig. 4c). A significant increase in surface sensible heat flux, due to increased surface temperature, contributes strongly to the reduced tropospheric cooling in these regions (Fig. 4d). There is little change in TOA LW cooling (Fig. 6e), whereas net downwelling LW radiation at the surface decreases (Fig. 6c). The net reduction in tropospheric cooling leads to reduced precipitation. The surface warming does not trigger enhanced moist convection, as seen over most tropical land regions. Cloud cover decreases significantly (Fig. 6b), which increases downwelling SW radiation at the surface and TOA (Figs. 6d,f). This enhances the land surface warming, causing further increases in upwelling LW and SH fluxes. The tropospheric cooling in the northeast of South America behaves similarly to the midlatitudes, though the dynamical mechanisms likely differ. This, coupled with a reduction in dry static energy

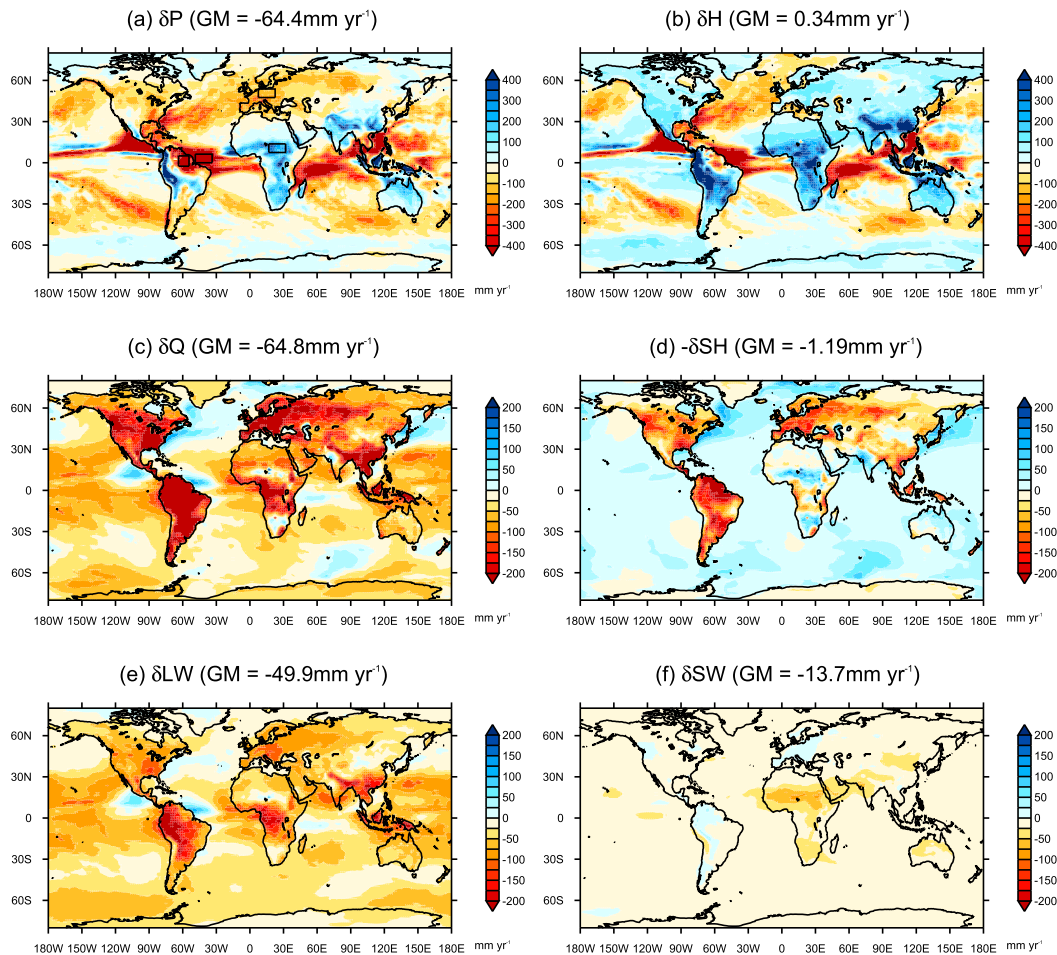


FIG. 4. Local energy budget changes for HadGEM2-A sstClim4xCO<sub>2</sub> simulation: (a) precipitation, (b) dry static energy flux divergence, (c) tropospheric diabatic cooling, (d) negative surface sensible heat flux, (e) LW cooling, and (f) SW cooling. All values are converted into precipitation units ( $\text{mm yr}^{-1}$ ), and blue represents positive contributions to precipitation in all panels. Global mean (GM) values are given for each panel. The boxes in (a) show the regions Europe, Africa, South America, and the Atlantic Ocean (for which the vertical profiles are analyzed in Fig. 7). Note that the color scale magnitude is larger for (a) and (b).

flux divergence, causes the reduction in precipitation observed there (discussed further in section 3d).

#### d. $4 \times \text{CO}_2$ tropospheric vertical profile

To help understand the tropospheric response in different regions to quadrupling CO<sub>2</sub>, we analyze the change in vertical profiles of temperature  $T$ , equivalent potential temperature  $\theta_e$ , relative humidity RH, and specific humidity  $q$  for HadGEM2-A, as shown in Fig. 7. The global mean response (Fig. 7a) is dominated by the response of the oceans (Fig. 7c). Tropospheric temperature change grows with height above the surface, with a maximum increase at 850 hPa and a corresponding reduction in relative humidity. This warming and drying around the upper part of the boundary layer inhibits vertical motion, stabilizing the atmosphere and reducing

precipitation. In contrast, over land the largest temperature increase is at the surface, specific humidity increases throughout most of the troposphere, and there is a weaker reduction in lower-tropospheric relative humidity than over the ocean (Fig. 7b). This pattern destabilizes the troposphere, enhancing convection and precipitation. Dong et al. (2009) observed similar differences in the rapid tropospheric response over land and sea to increased CO<sub>2</sub>.

The tropospheric response varies greatly between different regions, as seen in Figs. 7d–g (geographical locations of the regions are shown in Fig. 4a). Over central Africa, where precipitation increases significantly, the tropospheric temperature increases near the surface (Fig. 7d). This is accompanied by an increase in specific humidity at around 500–800 hPa. As a result,

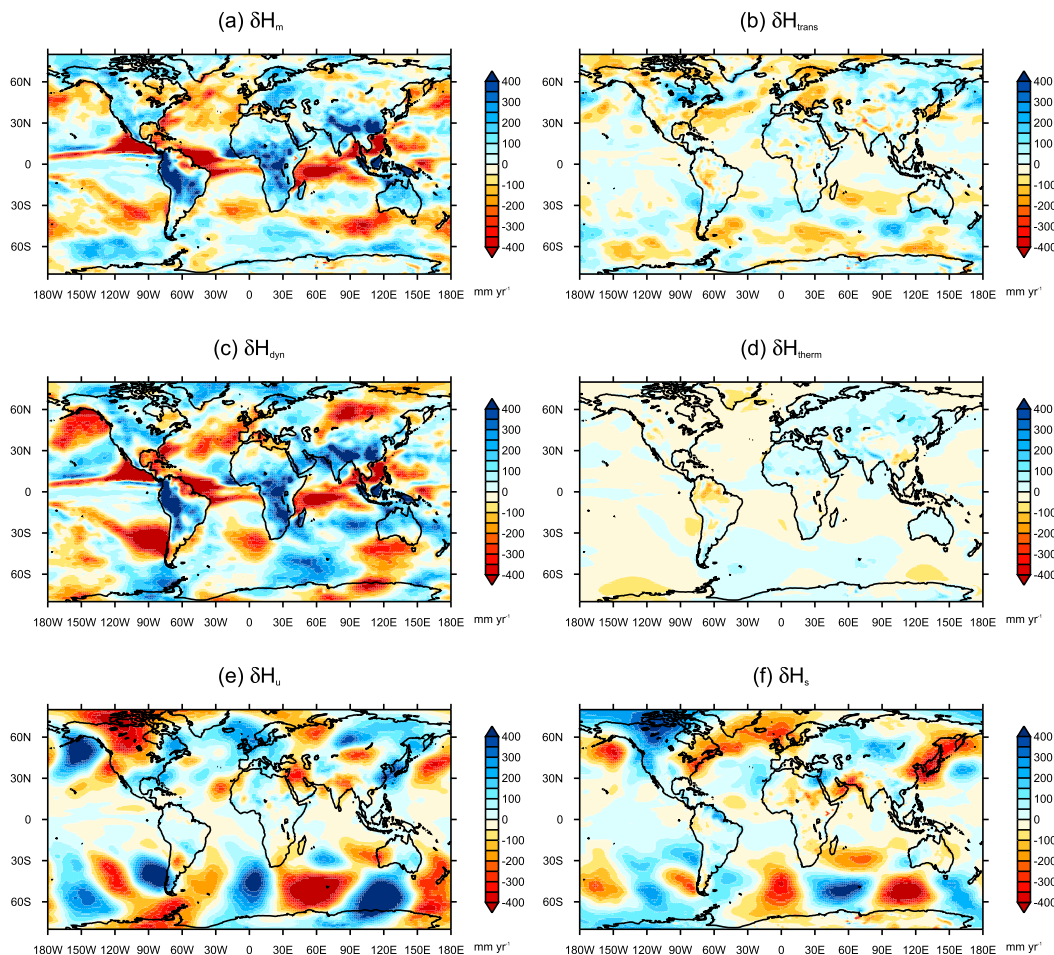


FIG. 5. (a) Mean  $H_m$  and (b) eddy  $H_{\text{trans}}$  components of the change in dry static energy flux divergence for HadGEM2-A sstClim4xCO<sub>2</sub> simulation. (c)–(f) The mean term decomposed into (c) dynamic  $H_{\text{dyn}}$ , (d) thermodynamic  $H_{\text{therm}}$ , (e) horizontal wind  $H_u$ , and (f) horizontal gradient  $H_s$  components, as outlined in Eqs. (2)–(4). All values are converted to precipitation units ( $\text{mm yr}^{-1}$ ), with blue representing a positive contribution to precipitation.

the equivalent potential temperature is significantly increased in the lower half of the troposphere, while temperature remains almost unchanged in the upper troposphere. This combination increases the deep convective instability and drives increased convection and precipitation. Over Europe, where precipitation decreases, the temperature increases throughout most of the troposphere, with a peak at around 900 hPa (Fig. 7e). Unlike over Africa, the specific humidity does not increase anywhere in the troposphere and decreases below 600 hPa. As a result, the relative humidity reduces significantly, causing a reduction in precipitation. This indicates that a lack of available moisture prevents enhanced moist convection, as seen over tropical land regions.

Figure 7f shows the tropospheric adjustment in a region of significantly reduced precipitation over the

tropical Atlantic. It can be seen that there is an increase in temperature between 850 and 500 hPa, which inhibits vertical motion. There is also a reduction in specific and relative humidity above 800 hPa. As a result, precipitation decreases considerably in this region. Figure 7g shows the tropospheric adjustment over northeastern South America, which responds differently to most tropical land regions, with a significant reduction in precipitation. The temperature increases near the surface, which would tend to destabilize the troposphere. However, there is a large reduction in moisture levels near the surface, causing a peak in equivalent potential temperature at around 850 hPa, and almost no change in the surface values. This pattern implies a lifted cloud base, which, combined with the warming just above the boundary layer, inhibits moist convection and reduces



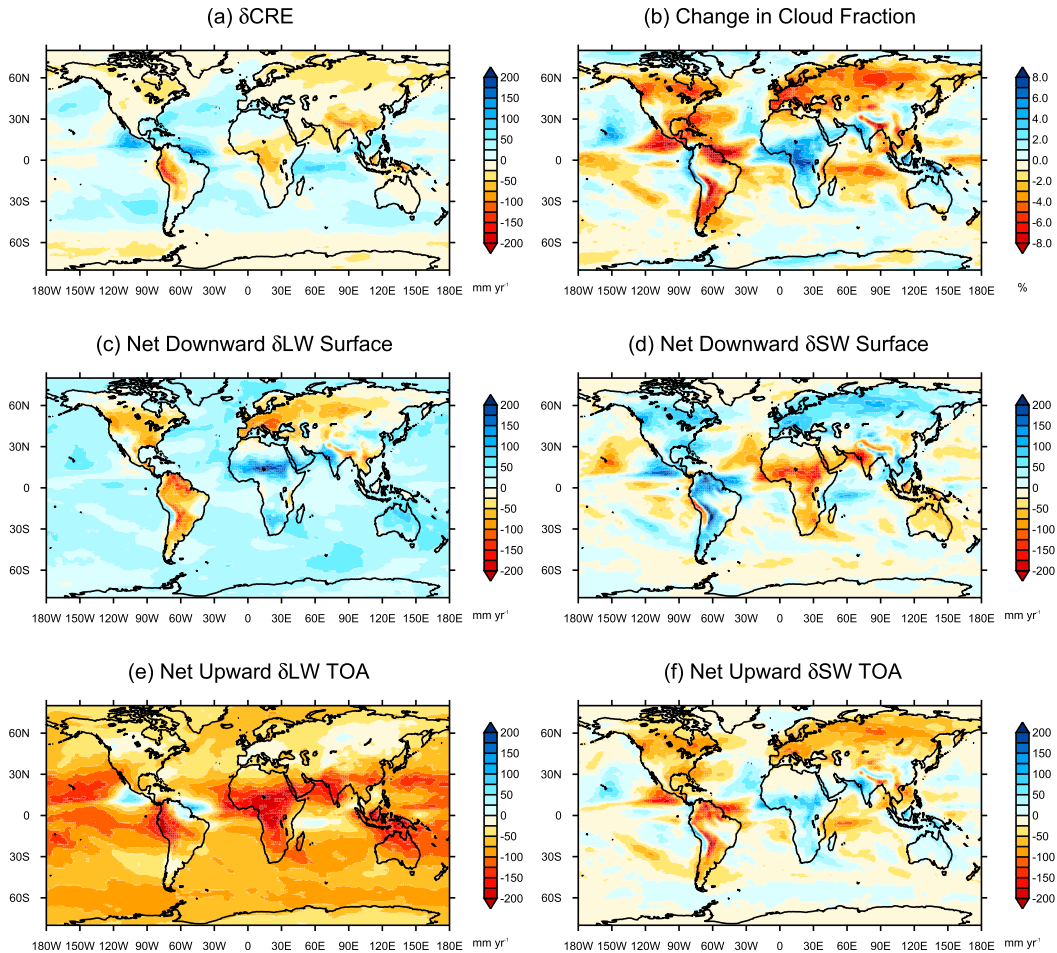


FIG. 6. HadGEM2-A sstClim4xCO<sub>2</sub> changes in (a) atmospheric CRE (mm yr<sup>-1</sup>), (b) total cloud fraction (%), (c) net downward LW radiation at the surface (mm yr<sup>-1</sup>), (d) net downward SW radiation at the surface (mm yr<sup>-1</sup>), (e) net upward LW radiation at the TOA (mm yr<sup>-1</sup>), and (f) net upward SW radiation at the TOA (mm yr<sup>-1</sup>). All radiative changes are converted to precipitation units (mm yr<sup>-1</sup>).

precipitation. Various studies have found that the physiological forcing of CO<sub>2</sub> significantly reduces evapotranspiration over the Amazonian basin (Andrews et al. 2011; Pu and Dickinson 2014). This occurs because, under increased CO<sub>2</sub> concentration, plant stomata do not open as wide. This likely contributes to the large reduction in humidity over South America.

#### 4. Conclusions

The rapid climate response to forcing can have important implications for long-term climate change (Andrews et al. 2010; Bony et al. 2013). In this study, we find that the spatial pattern of rapid precipitation adjustment due to forcing is primarily driven by the rapid land surface response, rather than the change in tropospheric diabatic cooling. As a result, the spatial pattern

due to quadrupling CO<sub>2</sub> opposes that due to increased sulfate or all anthropogenic aerosols. Increasing CO<sub>2</sub> levels causes warming of the land surface because of enhanced downwelling LW radiation. This destabilizes the atmosphere by warming the lower troposphere, producing an overall shift of convection and precipitation to over land. The opposite happens in response to aerosols: increased sulfate levels cool the land surface because of reduced downwelling SW radiation. This stabilizes the troposphere and reduces precipitation over land. The same effect occurs for an increase in all anthropogenic aerosol levels.

Current climate models exhibit a robust pattern of rapid precipitation change due to quadrupling CO<sub>2</sub>. This implies that the uncertainty in long-term predictions is mainly associated with the response to SST-mediated feedbacks. The most significant regional changes occur in the tropics, mainly because of circulation adjustments

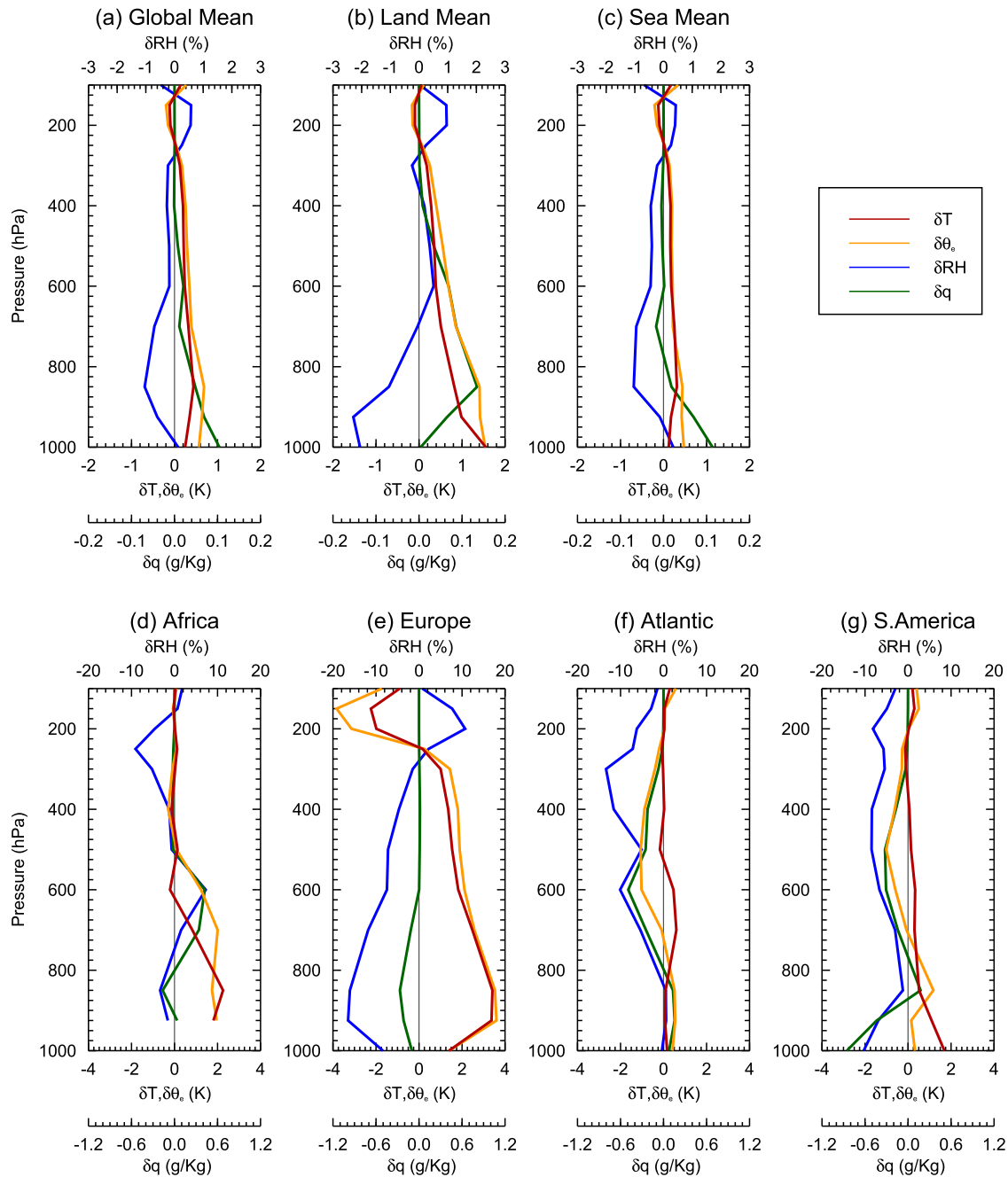


FIG. 7. HadGEM2-A vertical profile adjustment in temperature  $T$  (K), equivalent potential temperature  $\theta_e$  (K), relative humidity RH (%), and specific humidity  $q$  ( $\text{g Kg}^{-1}$ ) for (a) the global mean, (b) land mean, (c) sea mean, (d) a region of increased precipitation over Africa, (e) a region of decreased precipitation over Europe, (f) a region of decreased precipitation over the tropical Atlantic, and (g) a region of decreased precipitation over northeastern South America. The specific locations of the regions are shown in Fig. 4a.

associated with changes in vertical motions. Increased land surface temperature drives enhanced moist convection over central Africa, southern Asia, the Maritime Continent, and western South America. Over the tropical oceans, there are significant reductions in precipitation due to a weakening of overturning circulation

and a general shift of convection to over land. Increased tropospheric temperature, due to LW absorption by  $\text{CO}_2$ , above unchanged SST strongly inhibits vertical motion.

Over midlatitude land regions, the change in tropospheric cooling generally dominates the precipitation

TABLE A1. List of models analyzed for each simulation. An X indicates that the model was available, and a dash indicates that a model was not available. (Expansions of acronyms are available at <http://www.ametsoc.org/PubsAcronymList>.)

Model	sstClim4xCO <sub>2</sub>	sstClimSulfate	sstClimAerosol
BCC_CSM1.1	X	X	X
CanESM2	X	X	X
CCSM4	X	—	—
CESM1(CAM5)	X	—	—
CSIRO Mk3.6.0	X	X	X
FGOALS-s2	X	X	X
GFDL CM3	—	X	X
HadGEM2-A	X	X	X
INM-CM4.0	X	—	—
IPSL-CM5A-LR	X	X	X
MIROC5	X	X	X
MPI-ESM-LR	X	X	X
MPI-ESM-MR	X	—	—
MPI-ESM-P	X	—	—
MRI-CGCM3	X	X	X
NorESM1-M	X	—	X

response to CO<sub>2</sub>. Horizontal advection of dry static energy counteracts energy imbalances due to changes in vertical motions. This, combined with lower moisture levels, prevents enhanced moist convection. Reduced tropospheric cooling therefore leads to drying over many midlatitude land regions.

In the future it would be useful to investigate the rapid precipitation response to black carbon using a larger forcing, as the rapid adjustment can be larger than the feedback response (Andrews et al. 2010; Ming et al. 2010), and the forcing can vary depending on the height at which it is situated (Ban-Weiss et al. 2012). In addition, given the short time scale of rapid precipitation adjustments, higher-resolution convection-permitting models could be utilized for analysis. Convection-permitting models can improve simulations of convective circulations (Sato et al. 2009; Oouchi et al. 2009) and could improve our understanding of long-term climate change.

*Acknowledgments.* TBR was supported by an NERC Ph.D. Case Award with the Met Office, PMF was supported by a Royal Society Wolfson Merit Award and EPSRC Grant EP/I014721/1, and TA was supported by the Joint UK DECC/Defra Met Office Hadley Centre Climate Programme (GA01101). TBR would like to thank Øivind Hodnebrog for useful discussions on figure presentation. We acknowledge the World Climate Research Programme's Working Group on Coupled Modelling, which is responsible for CMIP, and we thank the climate modeling groups (listed in Table A1) for producing and making available their model output. For CMIP the U.S. Department of Energy's Program for Climate Model

Diagnosis and Intercomparison provides coordinating support and led development of software infrastructure in partnership with the Global Organization for Earth System Science Portals.

## APPENDIX

### List of Models

The list of models participating in CMIP5 from which the data were obtained is presented in Table A1.

### REFERENCES

- Allen, M. R., and W. J. Ingram, 2002: Constraints on future changes in climate and the hydrologic cycle. *Nature*, **419**, 224–232, doi:10.1038/nature01092.
- Allen, R. J., A. T. Evan, and B. B. Booth, 2015: Interhemispheric aerosol radiative forcing and tropical precipitation shifts during the late twentieth century. *J. Climate*, **28**, 8129–8246, doi:10.1175/JCLI-D-15-0148.1.
- Andrews, T., and P. M. Forster, 2010: The transient response of global-mean precipitation to increasing carbon dioxide levels. *Environ. Res. Lett.*, **5**, 025212, doi:10.1088/1748-9326/5/2/025212.
- , —, O. Boucher, N. Bellouin, and A. Jones, 2010: Precipitation, radiative forcing and global temperature change. *Geophys. Res. Lett.*, **37**, L14701, doi:10.1029/2010GL043991.
- , M. Doutriaux-Boucher, O. Boucher, and P. M. Forster, 2011: A regional and global analysis of carbon dioxide physiological forcing and its impact on climate. *Climate Dyn.*, **36**, 783–792, doi:10.1007/s00382-010-0742-1.
- Bala, G., K. Caldeira, and R. Nemani, 2010: Fast versus slow response in climate change: Implications for the global hydrological cycle. *Climate Dyn.*, **35**, 423–434, doi:10.1007/s00382-009-0583-y.
- Ban-Weiss, G. A., L. Cao, G. Bala, and K. Caldeira, 2012: Dependence of climate forcing and response on the altitude of black carbon aerosols. *Climate Dyn.*, **38**, 897–911, doi:10.1007/s00382-011-1052-y.
- Bony, S., G. Bellon, D. Klocke, S. Sherwood, S. Fermepin, and S. Denvil, 2013: Robust direct effect of carbon dioxide on tropical circulation and regional precipitation. *Nat. Geosci.*, **6**, 447–451, doi:10.1038/ngeo1799.
- Cao, L., G. Bala, and K. Caldeira, 2011: Why is there a short-term increase in global precipitation in response to diminished CO<sub>2</sub> forcing? *Geophys. Res. Lett.*, **38**, L06703, doi:10.1029/2011GL046713.
- , —, and —, 2012: Climate response to changes in atmospheric carbon dioxide and solar irradiance on the time scale of days to weeks. *Environ. Res. Lett.*, **7**, 034015, doi:10.1088/1748-9326/7/3/034015.
- Chadwick, R., P. Good, T. Andrews, and G. Martin, 2014: Surface warming patterns drive tropical rainfall pattern responses to CO<sub>2</sub> forcing on all timescales. *Geophys. Res. Lett.*, **41**, 610–615, doi:10.1002/2013GL058504.
- Dong, B., J. M. Gregory, and R. T. Sutton, 2009: Understanding land–sea warming contrast in response to increasing greenhouse gases. Part I: Transient adjustment. *J. Climate*, **22**, 3079–3097, doi:10.1175/2009JCLI2652.1.

- Emori, S., 2005: Dynamic and thermodynamic changes in mean and extreme precipitation under changed climate. *Geophys. Res. Lett.*, **32**, L17706, doi:[10.1029/2005GL023272](https://doi.org/10.1029/2005GL023272).
- Ganguly, D., P. J. Rasch, H. Wang, and J. Yoon, 2012: Fast and slow responses of the South Asian monsoon system to anthropogenic aerosols. *Geophys. Res. Lett.*, **39**, L18804, doi:[10.1029/2012GL053043](https://doi.org/10.1029/2012GL053043).
- Huang, P., S. Xie, K. Hu, G. Huang, and R. Huang, 2013: Patterns of the seasonal response of tropical rainfall to global warming. *Nat. Geosci.*, **6**, 357–361, doi:[10.1038/ngeo1792](https://doi.org/10.1038/ngeo1792).
- Kravitz, B., and Coauthors, 2013: An energetic perspective on hydrological cycle changes in the Geoengineering Model Intercomparison Project. *J. Geophys. Res.*, **118**, 13 087–13 102, doi:[10.1002/2013JD020502](https://doi.org/10.1002/2013JD020502).
- Kvalevåg, M. M., B. H. Samset, and G. Myhre, 2013: Hydrological sensitivity to greenhouse gases and aerosols in a global climate model. *Geophys. Res. Lett.*, **40**, 1432–1438, doi:[10.1002/grl.50318](https://doi.org/10.1002/grl.50318).
- Lambert, F. H., and N. E. Faull, 2007: Tropospheric adjustment: The response of two general circulation models to a change in insolation. *Geophys. Res. Lett.*, **34**, L03701, doi:[10.1029/2006GL028124](https://doi.org/10.1029/2006GL028124).
- , M. J. Webb, M. Yoshimori, and T. Yokohata, 2014: The cloud radiative effect on the atmospheric energy budget and global mean precipitation. *Climate Dyn.*, **44**, 2301–2325, doi:[10.1007/s00382-014-2174-9](https://doi.org/10.1007/s00382-014-2174-9).
- Liepert, B. G., and M. Previdi, 2012: Inter-model variability and biases of the global water cycle in CMIP3 coupled climate models. *Environ. Res. Lett.*, **7**, 014006, doi:[10.1088/1748-9326/7/1/014006](https://doi.org/10.1088/1748-9326/7/1/014006).
- Ma, J., and S.-P. Xie, 2013: Regional patterns of sea surface temperature change: A source of uncertainty in future projections of precipitation and atmospheric circulation. *J. Climate*, **26**, 2482–2501, doi:[10.1175/JCLI-D-12-00283.1](https://doi.org/10.1175/JCLI-D-12-00283.1).
- Ming, Y., V. Ramaswamy, and G. Persad, 2010: Two opposing effects of absorbing aerosols on global-mean precipitation. *Geophys. Res. Lett.*, **37**, L13701, doi:[10.1029/2010GL042895](https://doi.org/10.1029/2010GL042895).
- Mitchell, J., C. Wilson, and W. Cunnington, 1987: On CO<sub>2</sub> climate sensitivity and model dependence of results. *Quart. J. Roy. Meteor. Soc.*, **113**, 293–322, doi:[10.1256/smsqj.47516](https://doi.org/10.1256/smsqj.47516).
- Muller, C. J., and P. A. O’Gorman, 2011: An energetic perspective on the regional response of precipitation to climate change. *Nat. Climate Change*, **1**, 266–271, doi:[10.1038/nclimate1169](https://doi.org/10.1038/nclimate1169).
- O’Gorman, P. A., R. P. Allan, M. P. Byrne, and M. Previdi, 2012: Energetic constraints on precipitation under climate change. *Surv. Geophys.*, **33**, 585–608, doi:[10.1007/s10712-011-9159-6](https://doi.org/10.1007/s10712-011-9159-6).
- Oouchi, K., A. T. Noda, M. Satoh, B. Wang, S.-P. Xie, H. G. Takahashi, and T. Yasunari, 2009: Asian summer monsoon simulated by a global cloud-system-resolving model: Diurnal to intra-seasonal variability. *Geophys. Res. Lett.*, **36**, L11815, doi:[10.1029/2009GL038271](https://doi.org/10.1029/2009GL038271).
- Pendergrass, A. G., and D. L. Hartmann, 2014: The atmospheric energy constraint on global-mean precipitation change. *J. Climate*, **27**, 757–768, doi:[10.1175/JCLI-D-13-00163.1](https://doi.org/10.1175/JCLI-D-13-00163.1).
- Previdi, M., 2010: Radiative feedbacks on global precipitation. *Environ. Res. Lett.*, **5**, 025211, doi:[10.1088/1748-9326/5/2/025211](https://doi.org/10.1088/1748-9326/5/2/025211).
- Pu, B., and R. E. Dickinson, 2014: Hydrological changes in the climate system from leaf responses to increasing CO<sub>2</sub>. *Climate Dyn.*, **42**, 1905–1923, doi:[10.1007/s00382-013-1781-1](https://doi.org/10.1007/s00382-013-1781-1).
- Sato, T., H. Miura, M. Satoh, Y. N. Takayabu, and Y. Wang, 2009: Diurnal cycle of precipitation in the tropics simulated in a global cloud-resolving model. *J. Climate*, **22**, 4809–4826, doi:[10.1175/2009JCLI2890.1](https://doi.org/10.1175/2009JCLI2890.1).
- Sherwood, S. C., S. Bony, O. Boucher, C. Bretherton, P. M. Forster, J. M. Gregory, and B. Stevens, 2014: Adjustments in the forcing-feedback framework for understanding climate change. *Bull. Amer. Meteor. Soc.*, **96**, 217–228, doi:[10.1175/BAMS-D-13-00167.1](https://doi.org/10.1175/BAMS-D-13-00167.1).
- Soden, B. J., A. J. Broccoli, and R. S. Hemler, 2004: On the use of cloud forcing to estimate cloud feedback. *J. Climate*, **17**, 3661–3665, doi:[10.1175/1520-0442\(2004\)017<3661:OTUOCF>2.0.CO;2](https://doi.org/10.1175/1520-0442(2004)017<3661:OTUOCF>2.0.CO;2).
- Stephens, G. L., and Coauthors, 2010: Dreary state of precipitation in global models. *J. Geophys. Res.*, **115**, D24211, doi:[10.1029/2010JD014532](https://doi.org/10.1029/2010JD014532).
- Stevens, B., and S. Bony, 2013: What are climate models missing? *Science*, **31**, 1053–1054, doi:[10.1126/science.1237554](https://doi.org/10.1126/science.1237554).
- Taylor, K. E., R. J. Stouffer, and G. A. Meehl, 2009: A summary of the CMIP5 experiment design. WCRP Tech. Rep., 33 pp. [Available online at [http://cmip-pcmdi.llnl.gov/cmip5/docs/Taylor\\_CMIP5\\_design.pdf](http://cmip-pcmdi.llnl.gov/cmip5/docs/Taylor_CMIP5_design.pdf).]
- Wake, B., 2013: Flooding costs. *Nat. Climate Change*, **3**, 778–778, doi:[10.1038/nclimate1997](https://doi.org/10.1038/nclimate1997).
- Xie, S.-P., B. Lu, and B. Xiang, 2013: Similar spatial patterns of climate responses to aerosol and greenhouse gas changes. *Nat. Geosci.*, **6**, 828–832, doi:[10.1038/ngeo1931](https://doi.org/10.1038/ngeo1931).